Struct Multidisc Optim (2007) 33: 47–59
DOI 10.1007/s00158-006-0031-0

RESEARCH PAPER

Marco Rovati · Daniele Veber

Optimal topologies for micropolar solids

Received: 5 October 2005 / Revised manuscript received: 2 March 2006 / Published online: 28 September 2006

Abstract Micropolar field theory represents an extension of the classical Cauchy continuum theory. In this paper, a topology optimization procedure for maximum stiffness is applied to structural elements made of micropolar (Cosserat) solids. Some special problems are dealt with and particular attention is given to models that refer to structural interfaces. The results are in good agreement with the real behavior of some biological tissues.

Keywords Topology optimization · Micropolar continua · Cosserat theory · Structural interfaces

1 Introduction

Conventional continuum mechanics approaches cannot incorporate any intrinsic material length scale. However, real materials often exhibit a number of important length scales, which must be included in any realistic model: grains, particles, fibers, cellular solids, and biological tissues. So-called nonlocal theories can be used to account for size effects in the mechanical behavior of materials. The departure from local theories begins with the micropolar (or Cosserat) continuum. A Cosserat medium is a continuous collection of particles that behaves like rigid bodies. Accordingly, each material point is endowed with translational and rotational degrees of freedom that describe its displacement and the rotation of an underlying microstructure. Dealing with two-dimensional bodies, the objective of the paper is to find the optimal distribution of a given amount of material in a fixed design domain with prescribed boundary conditions to minimize the global structural compliance. The problem is based on a suitable parametrization of the constitutive tensor in terms of the material density function (see Eschenauer and Olhoff 2001).

In Section 2, the basic equations governing the kinematics, equilibrium, and constitutive behavior of a micropolar continuum are briefly recalled. Section 3 deals with two-dimensional problems for isotropic Cosserat solids. The computational aspects of the problem are dealt with in Section 4 through a suitable finite element formulation for Cosserat solids. The optimization procedure follows the Solid Isotropic Material with Penalization (SIMP; Bendsøe and Sigmund 2002) model. A comparison among different models of material interpolation is made. In particular, a modified SIMP model is adopted to take into account both translational and rotational constitutive tensors.

Examples of application will be presented in Section 5 with reference to a cantilever beam and to structural interface problems, as can appear in biological structures like bone tissues and cartilages. The dependence of the optimal solutions on the length scale, coupling number, and on the differences from classical elasticity are also pointed out.

2 The mechanical model

In this section, the basic equations for micropolar elasticity are briefly reviewed (for more details, see Eringen 1999, 1966; Novacki 1986). The main difference between the classical (Cauchy) elasticity theory and nonlocal theories consists in the basic idea to establish a relationship between macroscopic and microscopic mechanical quantities in materials with microstructure. Continuum nonlocal models can be classified into three main groups, namely, integral models, higher order gradient models, and micropolar theories (see Fatemi et al. 2002).

The fundamental distinction between classical elasticity and higher order gradient elasticity theories lies in the nature of interactions of material elements. Microcontinuum field theories can be classified according to the kinematical degrees of freedom associated with each material particle. These classes refer to the micromorphic theory, microstructure

M. Rovati · D. Veber (✉)
Department of Mechanical and Structural Engineering,
University of Trento, Via Mesiano 77, Trento, Italy
Tel.: +39-0461-882523
Fax: +39-0461-882599
e-mail: daniele.veber@ing.unitn.it

theory, micropolar and Cosserat theory, and the couple stress theory (see Chen et al. 2004).

In the next subsections, the governing equations for a three-dimensional micropolar continuum body Ω, with boundary $\partial\Omega$, are given in index notation (with $i, j, k, l, m, n = 1, 2, 3$). The usual rule of summation over a repeated index is assumed and the comma indicates the partial derivative with respect to the relevant variable.

2.1 Kinematics

The kinematics of a micropolar continuum is characterized by introducing an additional deformation field produced by microrotations. These microrotations are independent of the displacement field u_k (see Fig. 1 in a two-dimensional representation). The vector of microrotations is defined as ϕ_m, and u_k is the displacement vector. The micropolar strain tensor ε_{kl} is defined as a function of the displacement and microrotation fields:

$$\varepsilon_{kl} = e_{kl} + \mathrm{e}_{klm}\left(w_m - \phi_m\right), \qquad \text{in } \overline{\Omega}, \tag{1}$$

where e_{kl} denotes the macrostrain tensor:

$$e_{kl} = \frac{1}{2}\left(u_{k,l} + u_{l,k}\right), \qquad \text{in } \overline{\Omega}. \tag{2}$$

$\overline{\Omega} = \Omega \cup \partial\Omega$ is the closure of the domain.

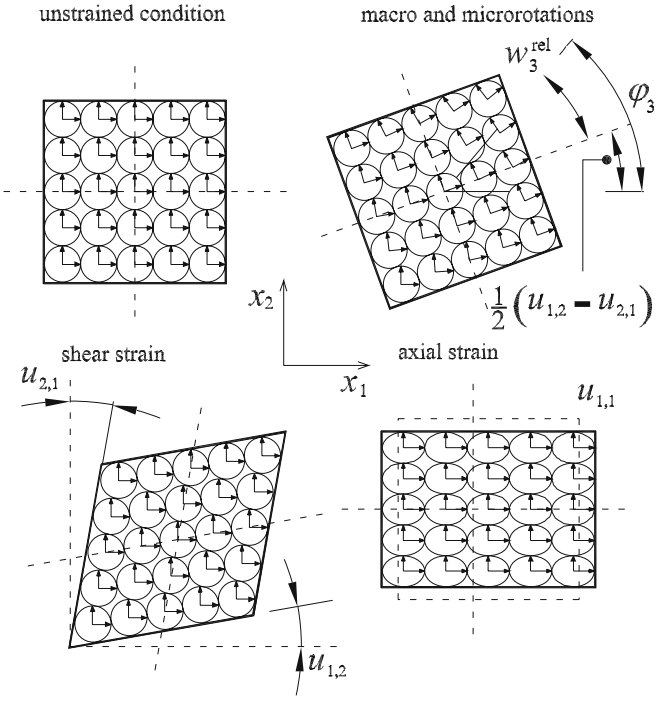

Fig. 1 Kinematical model of an infinitesimal plane element

The macroscopic rotation tensor describes the rigid body rotation of the classical elasticity theory through the rotation vector w_m (as w_3 in Fig. 1):

$$\mathrm{e}_{klm} w_m = \frac{1}{2}\left(u_{l,k} - u_{k,l}\right), \qquad \text{in } \overline{\Omega}; \tag{3}$$

where e_{klm} is the permutation tensor.

In the micropolar theory, the relative rotation between the material element and the corresponding microrotation is represented by:

$$\mathrm{w}_k^{rel} = w_k - \phi_k. \tag{4}$$

Finally, the microcurvature tensor or microrotation gradient is defined as follows:

$$\chi_{kl} = \phi_{l,k}. \tag{5}$$

Note that in the symbolic representation of Fig. 1 the macrorotation is given by a rigid body motion of the infinitesimal plane element, whereas the microrotations are due to rotations of the material particles inside that element. The microcurvatures correspond to the microrotation gradient, i.e., the relative rotations between the material particles of the element.

2.2 Equilibrium

The higher order gradient theories necessitate the introduction of additional stress tensors, which are conjugate to the additional deformation measures (e.g., couple or moment stresses in the Cosserat type theories and double forces tensor in the Mindlin continuum; see Chen et al. 2004). In the elasticity theories, these new stress tensors can normally be obtained by differentiating the variation of a total elastic potential (i.e., the elastic energy density) with respect to the deformation measures. In Cartesian coordinates, the equilibrium equations for (generally asymmetric) stresses σ_{ji} and couple stresses m_{ji} are:

$$\sigma_{ji,j} + \mathrm{b_i} = 0, \qquad \text{in } \Omega, \tag{6}$$

$$m_{ji,j} + \mathrm{e}_{ilk}\sigma_{lk} + \mathrm{m}_i = 0, \qquad \text{in } \Omega, \tag{7}$$

where b_i is the body forces and m_i is the body couples (see Figs. 2 and 3 for two-dimensional representations).

2.3 Constitutive equations

The constitutive equations for a micropolar linear (in general anisotropic) elastic solid are given by (Lakes and Benedict 1982):

$$\sigma_{ij} = E_{ijkl}\varepsilon_{kl} + B_{ijkl}\chi_{kl}, \tag{8}$$

$$m_{ij} = B_{klij}\varepsilon_{kl} + K_{ijkl}\chi_{kl}, \tag{9}$$

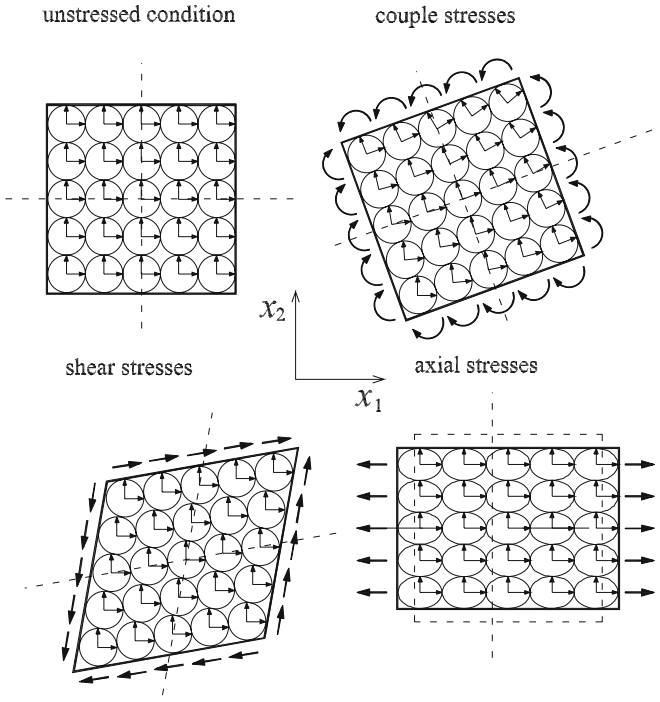

Fig. 2 Statical model of an infinitesimal plane element

in $\overline{\Omega}$, where E_{ijkl}, B_{ijkl}, and K_{ijkl} are the micropolar fourth rank stiffness tensors. E_{ijkl} associates stresses with strains and K_{ijkl} associates couple stresses with microrotations. B_{ijkl} is often called "pseudotensor" in the sense that it vanishes in the case of isotropic micropolar material. This tensor is responsible of the coupling between stresses and microcurvatures and between couple stresses and strains. Moreover,

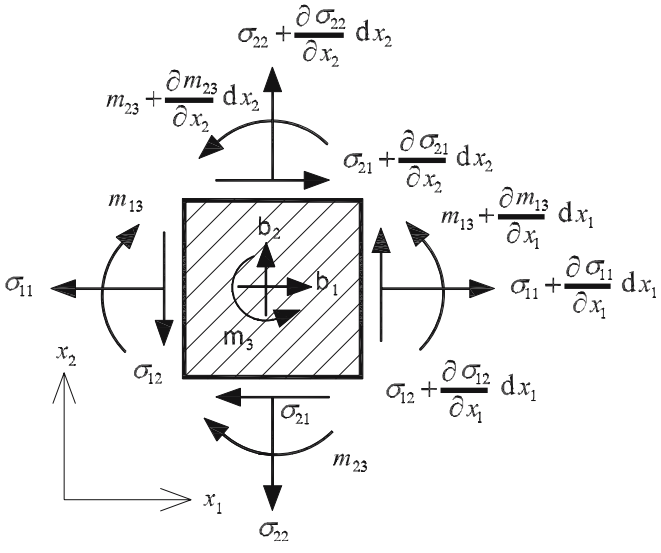

Fig. 3 Stresses and couple stresses on an infinitesimal plane element at equilibrium

it must be noticed that E_{ijkl} and K_{ijkl} enjoy the major symmetries $E_{ijkl} = E_{klij}$ and $K_{ijkl} = K_{klij}$ because both tensors are associated with a potential energy. Conversely, the minor symmetries are not ensured because of the presence of asymmetric total strain and microcurvature tensors.

In the case of a micropolar isotropic linearly elastic solid, (8) and (9) are reduced to:

$$\sigma_{kl} = \lambda e_{nn}\delta_{kl} + (2\mu + \kappa)\, e_{kl} + \kappa \mathrm{e}_{klm}(w_m - \phi_m), \tag{10}$$

$$m_{kl} = \alpha \phi_{n,n}\delta_{kl} + \gamma \phi_{l,k} + \beta \phi_{k,l}\,, \tag{11}$$

in Ω. In the last two expressions, λ and μ denote the Lamè constants of the classical isotropic elasticity theory, whereas $\mu^* = \mu - \kappa/2$ is the micropolar shear modulus (Rosenberg and Cimrman 2001). Moreover, κ, α, β, and γ are micropolar constants that vanish when the classical elasticity theory is recovered.

2.4 Boundary conditions and total potential energy

The boundary of the body is decomposed in two parts $\partial\Omega = \partial\Omega_l \cup \partial\Omega_c$. On the first part, the classical conditions on surface tractions hold:

$$\mathrm{t}_j = \sigma_{ij} n_i\,, \qquad \text{on } \partial\Omega_l \tag{12}$$

and, in addition, an analogous condition for the surface couples must be fulfilled:

$$\mathrm{s}_j = m_{ij} n_i\,, \qquad \text{on } \partial\Omega_l. \tag{13}$$

On the second part of the boundary the following conditions hold:

$$\phi_j = \phi_j^0\,, \qquad \text{on } \partial\Omega_c, \tag{14}$$

$$u_j = u_j^0\,, \qquad \text{on } \partial\Omega_c, \tag{15}$$

where ϕ_j^0 and u_j^0 are prescribed microrotations and displacements vectors. Then, the total potential energy for a Cosserat elastic body can be written as:

$$\Pi = \frac{1}{2}\int_\Omega \left(\sigma_{ij}\varepsilon_{ij} + m_{ij}\chi_{ij}\right)\, d\Omega - \int_\Omega \left(\mathrm{b}_j u_j + \mathrm{m}_j \phi_j\right)\, d\Omega - \int_{\partial\Omega} \left(\mathrm{t}_j u_j + \mathrm{s}_j \phi_j\right)\, dS \tag{16}$$

and the strain energy density, written in terms of Lamè constants, reads:

$$\Psi = \frac{1}{2}\left[\lambda \varepsilon_{kk}\varepsilon_{ll} + (2\mu + \kappa)\,\varepsilon_{kl}\varepsilon_{kl}\right] + \kappa\,(w_k - \phi_k)\,(w_k - \phi_k) + \frac{1}{2}\left(\gamma \phi_{k,l}\phi_{k,l}\right). \tag{17}$$

3 Two-dimensional case

Referring to a plane problem, in the Cartesian plane, x_1x_2, the kinematics of the body is described through the components u_1 and u_2 of the displacement vector $\mathbf{u}$, together with the third component ϕ_3 of the microrotation vector $\boldsymbol{\phi}$, as follows:

$$\varepsilon_{11} = u_{1,1}\,, \qquad \varepsilon_{22} = u_{2,2}\,,$$
$$\varepsilon_{12} = u_{2,1} - \phi_3\,, \quad \varepsilon_{21} = u_{1,2} + \phi_3. \tag{18}$$

The components of the microcurvature tensor read:

$$\chi_{13} = \phi_{3,1}\,, \qquad \chi_{23} = \phi_{3,2}. \tag{19}$$

In two dimensions, the equilibrium equations are reduced to:

$$\sigma_{11,1} + \sigma_{21,2} + \mathrm{b}_1 = 0\,,$$
$$\sigma_{12,1} + \sigma_{22,2} + \mathrm{b}_2 = 0\,,$$
$$\sigma_{12} - \sigma_{21} + m_{13,1} + m_{23,2} + \mathrm{m}_3 = 0. \tag{20}$$

When the constitutive equations are considered, it is necessary to distinguish between plane strain and plane stress conditions. In the case of the plane strain, one has:

$$\sigma_{11} = e_{11}(\lambda + 2\mu + \kappa) + e_{22}(\lambda),$$
$$\sigma_{22} = e_{22}(\lambda + 2\mu + \kappa) + e_{11}(\lambda),$$
$$\sigma_{12} = e_{12}\,(2\mu + \kappa) + \kappa(w_3 - \phi_3),$$
$$\sigma_{21} = e_{21}\,(2\mu + \kappa) - \kappa\,(w_3 - \phi_3)\,,$$
$$m_{13} = \gamma\phi_{3,1}\,, \qquad m_{23} = \gamma\phi_{3,2}\,, \tag{21}$$

whereas in the plane stress case:

$$\sigma_{11} = e_{11}(\lambda + 2\mu + \kappa) + (\lambda)\,(e_{22} + e_{33})\,,$$
$$\sigma_{22} = e_{22}(\lambda + 2\mu + \kappa) + (\lambda)(e_{11} + e_{33}),$$
$$\sigma_{12} = e_{12}\,(2\mu + \kappa) + \kappa\,(w_3 - \phi_3)\,,$$
$$\sigma_{21} = e_{21}\,(2\mu + \kappa) - \kappa\,(w_3 - \phi_3)\,,$$
$$m_{13} = \gamma\phi_{3,1}\,, \qquad m_{23} = \gamma\phi_{3,2}\,, \tag{22}$$

where:

$$e_{33} = -\,(e_{11} + e_{22})\,\frac{\lambda}{(\lambda + 2\mu + \kappa)}. \tag{23}$$

Commonly, generalized engineering constants are adopted (which are six in 3-D and four in 2-D). In two dimensions (Novacki 1986), in addition to the usual Young's modulus and Poisson's ratio defined respectively as

$$E_m = \frac{(2\mu + \kappa)(3\lambda + 2\mu + \kappa)}{2\mu + 2\lambda + \kappa} = E \tag{24}$$

and

$$\nu_m = \frac{\lambda}{2\mu + 2\lambda + \kappa} = \nu\,, \tag{25}$$

there are two additional parameters. These are the characteristic length for bending,

$$\ell_m = \left(\frac{\gamma}{4\,\mu + 2\kappa}\right)^{1/2} = \left(\frac{\gamma\,(1+\nu)}{2\,E}\right)^{1/2} \tag{26}$$

and the so-called "coupling number"

$$N_m = \left(\frac{\kappa}{2\mu + 2\kappa}\right)^{1/2} = \left(\frac{\kappa\,(1+\nu)}{E + \kappa\,(1+\nu)}\right)^{1/2}. \tag{27}$$

Note that when $N_m = 0$ and $\ell_m = 0$, the classical Cauchy theory is recovered. The characteristic length can be shown to be directly related to Cosserat effects in plane strain bending of a slab (Gauthier and Jahsman 1975). Experimental determination of such a length was provided by Lakes (Lakes 1986) for porous materials. To fulfill thermodynamics requirements, these constants must satisfy the following bounds (referring again to the plane case, see Eringen 1966; Lakes and Benedict 1982):

$$0 < \ell_m^2 < \infty\,, \tag{28}$$

$$0 < E_m < \infty\,, \tag{29}$$

and:

$$-1 < \nu_m < 1 \text{ (in 2-D)}, \quad \frac{1}{2} \text{ (in 3-D)}. \tag{30}$$

Finally, the bounds on N_m are:

$$0 < N_m^2 < 1. \tag{31}$$

In the plane case, again, the total potential energy takes the form:

$$\begin{aligned}\Pi = {} & \frac{1}{2}\int_\Omega (\sigma_{11}\varepsilon_{11} + \sigma_{22}\varepsilon_{22} + \sigma_{12}\varepsilon_{12} + \sigma_{21}\varepsilon_{21})\; d\Omega \\ & + \frac{1}{2}\int_\Omega (m_{13}\chi_{13} + m_{23}\chi_{23})\; d\Omega \\ & - \int_\Omega (\mathrm{b}_1 u_1 + \mathrm{b}_2 u_2 + \mathrm{m}_3\phi_3)\; d\Omega \\ & - \int_{\partial\Omega} (\mathrm{t}_1 u_1 + \mathrm{t}_2 u_2 + \mathrm{s}_3\phi_3)\; dS. \end{aligned} \tag{32}$$

4 The topology optimization problem

4.1 Problem formulation

In this paper the classical problem of maximum global stiffness [or minimum compliance $\mathcal{C} = l(\mathbf{u}) + g(\boldsymbol{\phi})$, see (33) below] is dealt with, referring to micropolar solids. The

problem reads (see Bendsøe and Sigmund 2002 and the references therein):

$$\min_{\rho,u,\phi} \mathcal{C}(E_{ijkl}(\rho), K_{ijkl}(\rho)) \qquad \text{according to :}$$

$$E_{ijkl} \in \mathcal{E}_{adm}, \qquad K_{ijkl} \in \mathcal{K}_{adm},$$

subject to

$$\int_\Omega \rho \, d\Omega \le \mathcal{V}, \qquad 0 < \rho_{min} < \rho \le 1,$$

$$a_E(\underline{\mathbf{u}}, \underline{\bar{\mathbf{u}}}) + a_B(\underline{\mathbf{u}}, \underline{\bar{\mathbf{u}}}) + a_K(\underline{\mathbf{u}}, \underline{\bar{\mathbf{u}}}) = l(\bar{\mathbf{u}}) + g(\bar{\phi}),$$

$$\text{for all} \quad \bar{\mathbf{u}} \in U \quad \text{and} \quad \bar{\phi} \in S, \quad \text{where} \quad \underline{\mathbf{u}}^T = [\mathbf{u}, \phi]\,. \tag{33}$$

In (33), ρ denotes the material density and ρ_{min} is its lower limit introduced to avoid singularities in the finite element solution procedure. $\mathcal{V}$ is an upper bound on the total resource of material available. $\mathcal{E}_{adm}$ and $\mathcal{K}_{adm}$ are the sets of thermodynamically admissible micropolar stiffness tensors (Walsh and Tordesillas 2003). Moreover, U and S denote the space of the kinematically admissible displacement and the space of the kinematically admissible microrotation fields, respectively. The equilibrium equation is written in weak variational form.

$$\begin{aligned}
a_E(\mathbf{u}, \bar{\mathbf{u}}) &= \int_\Omega E_{ijkl}\varepsilon_{ij}(\mathbf{u})\varepsilon_{kl}(\bar{\mathbf{u}})\, d\Omega \\
a_B(\mathbf{u}, \bar{\mathbf{u}}, \phi, \bar{\phi}) &= \int_\Omega B_{ijkl}\varepsilon_{ij}(\bar{\mathbf{u}})\chi_{kl}(\phi)\, d\Omega \\
&\quad + \int_\Omega B_{klij}\varepsilon_{kl}(\mathbf{u})\chi_{ij}(\bar{\phi})\, d\Omega \\
a_K(\phi, \bar{\phi}) &= \int_\Omega K_{ijkl}\chi_{ij}(\phi)\chi_{kl}(\bar{\phi})\, d\Omega, \\
l\mathbf{u} &= \int_\Omega \mathrm{b_i} u_i \, d\Omega + \int_{\partial\Omega} \mathrm{t_i} u_i \, dS, \\
g(\phi) &= \int_\Omega \mathrm{m_i}\phi_i d\Omega + \int_{\partial\Omega} \mathrm{s_i}\phi_i dS.
\end{aligned} \tag{34}$$

In the following, for simplicity, b_i and m_i are assumed to be equal to zero vectors. In (34), a_E is a bilinear form, corresponding to the internal virtual translational work; a_K is a bilinear form, corresponding to the internal virtual rotational work, whereas a_B is responsible for the coupled virtual work of the two primary fields. The constrained minimization problem (33) can be rewritten as the search for stationarity of the augmented functional:

$$\begin{aligned}
\mathcal{L} &= l(\mathbf{u}) + g(\phi) - \bar{\lambda}\,[a_E(\mathbf{u}, \bar{\mathbf{u}}) + a_K(\phi, \bar{\phi}) \\
&\quad + a_B(\mathbf{u}, \bar{\mathbf{u}}, \phi, \bar{\phi}) - l(\bar{\mathbf{u}}) - g(\bar{\phi})] \\
&\quad + \Lambda\left(\int_\Omega \rho(x)\, d\Omega - \mathcal{V}\right) + \int_\Omega \lambda^+(x)\,(\rho(x) - 1)\, d\Omega \\
&\quad + \int_\Omega \lambda^-(x)\,(\rho_{min} - \rho)\, d\Omega,
\end{aligned} \tag{35}$$

where $\bar{\lambda}$ is the Lagrangian multiplier associated with the equality constraint and Λ, λ^+, and λ^- are the multipliers associated with inequalities. The necessary (Kuhn–Tucker) stationarity conditions for the Lagrangian functional $\mathcal{L}$ at equilibrium are:

$$\begin{aligned}
\frac{\partial \mathcal{L}}{\partial \rho} &= \frac{\partial E_{ijkl}}{\partial \rho}\,\varepsilon_{ij}(\mathbf{u})\,\varepsilon_{kl}(\mathbf{u}) + 2\,\frac{\partial B_{ijkl}}{\partial \rho}\,\varepsilon_{ij}(\mathbf{u})\,\chi_{kl}(\phi) \\
&\quad + \frac{\partial K_{ijkl}}{\partial \rho}\chi_{ij}(\phi)\,\chi_{kl}(\phi) - \Lambda - \lambda^+ + \lambda^- = 0\,,
\end{aligned} \tag{36}$$

$$\lambda^+\,(\rho(\mathbf{x}) - 1) = 0\,, \qquad \lambda^+ \ge 0\,, \tag{37}$$

$$\lambda^-\,(\rho_{min} - \rho(\mathbf{x})) = 0\,, \qquad \lambda^- \ge 0. \tag{38}$$

4.2 The modified Solid Isotropic Material with Penalization method

The power-law (or SIMP method) is a simple approach that allows one to obtain optimal designs consisting in regions inside a prescribed design space with the presence of isotropic material or absence of material (void).

Here, we adopted a modified SIMP model that takes into account different material interpolation laws for the translational, rotational, and "pseudo" micropolar stiffness tensors E_{ijkl}, K_{ijkl}, and B_{ijkl}. The moduli can be expressed as:

$$E_{ijkl}(\mathbf{x}) = \rho(\mathbf{x})^p E^0_{ijkl}\,, \qquad \text{with } p \ge 1\,, \tag{39}$$

$$K_{ijkl}(\mathbf{x}) = \rho(\mathbf{x})^q K^0_{ijkl}\,, \tag{40}$$

$$B_{ijkl}(\mathbf{x}) = \rho(\mathbf{x})^r B^0_{ijkl}\,, \tag{41}$$

where E^0_{ijkl}, K^0_{ijkl}, and B^0_{ijkl} are the constitutive tensors of the base material (see Figs. 4 and 5).

The stationarity conditions for the Lagrangian functional, when the SIMP method is adopted and if the side constraints are supposed to be inactive, read:

$$\begin{aligned}
&p\rho(\mathbf{x})^{p-1} E^0_{ijkl}\varepsilon_{ij}(\mathbf{u})\varepsilon_{kl}(\mathbf{u}) \\
&+ 2r\rho(\mathbf{x})^{r-1} B^0_{ijkl}\varepsilon_{ij}(\mathbf{u})\chi_{kl}(\boldsymbol{\phi}) \\
&+ q\rho(\mathbf{x})^{q-1} K^0_{ijkl}\chi_{ij}(\boldsymbol{\phi})\chi_{kl}(\boldsymbol{\phi}) = \Lambda.
\end{aligned} \tag{42}$$

The updating method for the design variable ρ is:

$$\rho_{k+1} = \begin{cases} \max\,[(1-\zeta)\ \rho_k, \rho_{min}]\,, \\ \qquad \text{if} \rho_k B_k^\eta \le \max\,[(1-\zeta)\ \rho_k, \rho_{min}]\,, \\ \min\,[(1+\zeta)\ \rho_k, 1]\,, \\ \qquad \text{if} \rho_k B_k^\eta \ge \min\,[(1+\zeta)\ \rho_k, 1]\,, \\ \rho_k B_k^\eta \quad \text{otherwise}, \end{cases} \tag{43}$$

where ρ_k is the material density at the kth iteration and B_k is given by (Cheng and Olhoff 1982):

$$B_k = \Lambda_k^{-1} \left[p\rho(\mathbf{x})^{p-1} E^0_{ijkl} \varepsilon_{ij}(\mathbf{u_k}) \varepsilon_{kl}(\mathbf{u_k}) + 2r\rho(\mathbf{x})^{r-1} B^0_{ijkl} \varepsilon_{ij}(\mathbf{u_k}) \chi_{kl}(\boldsymbol{\phi}_k) + q\rho(\mathbf{x})^{q-1} K^0_{ijkl} \chi_{ij}(\boldsymbol{\phi}_k) \chi_{kl}(\boldsymbol{\phi}_k) \right]. \quad (44)$$

At the optimum, B_k is equal to unity (see (42)). In the updating scheme (43), the variables η and ζ control the stability of the change of density at each iteration step. The variable η is a damping factor and ζ is the move limit for the density (Bendsøe and Sigmund 2002).

4.3 Finite element implementation

The finite element formulation is based on the stationarity of the total potential energy to find the discretized equilibrium equation. The discretized form of the total potential energy is:

$$\Pi = \frac{1}{2} \sum_{e=1}^{N} \left[(\mathbf{U}^e)^T \mathbf{K}^e_D \mathbf{U}^e + (\mathbf{U}^e)^T \mathbf{K}^e_R \mathbf{U}^e \right] - \sum_{e=1}^{N} \left[(\mathbf{F}^e)^T \mathbf{U}^e_D + (\mathbf{M}^e)^T \mathbf{U}^e_R \right], \quad (45)$$

where N is the number of finite elements

In the previous expression of the energy, the subscripts D and R refer to the translational and rotational parts of the generalized displacement vector, respectively. In the plane case the vector $\mathbf{U}$ reads:

$$\mathbf{U} = [\mathbf{U}_D, \mathbf{U}_R] = [u^a_1, \cdots, u^a_2, \cdots, \phi^a_3, \cdots]. \quad (46)$$

The displacement and microrotation fields in each finite element are approximated as functions of the nodal displacements and rotations through interpolation functions.

$$\mathbf{u} = [\, N^u \,] \mathbf{U}_D \,, \qquad \boldsymbol{\phi} = [\, N^\phi \,] \mathbf{U}_R \,, \quad (47)$$

where $[\, N^u \,]$ and $[\, N^\phi \,]$ are the matrices of the above-mentioned interpolation functions.

The global system of the discrete equilibrium equation is obtained through the standard finite element assembly technique:

$$\begin{bmatrix} \mathbf{K^{DD}} & \mathbf{K^{DR}} \\ \mathbf{K^{RD}} & \mathbf{K^{RR}} \end{bmatrix} \begin{bmatrix} \mathbf{U^D} \\ \mathbf{U^R} \end{bmatrix} = \begin{bmatrix} \mathbf{F} \\ \mathbf{M} \end{bmatrix}.$$

The finite elements adopted in the examples presented in Section 5 are the four-node generalized isoparametric finite element and the eight-node generalized isoparametric finite element. Each node has three degrees of freedom (two displacements and one microrotation). $\mathbf{F}$ and $\mathbf{M}$ are the nodal force and moment vectors. In the isotropic case, the micropolar stiffness pseudotensor B_{ijkl} is equal to the null tensor.

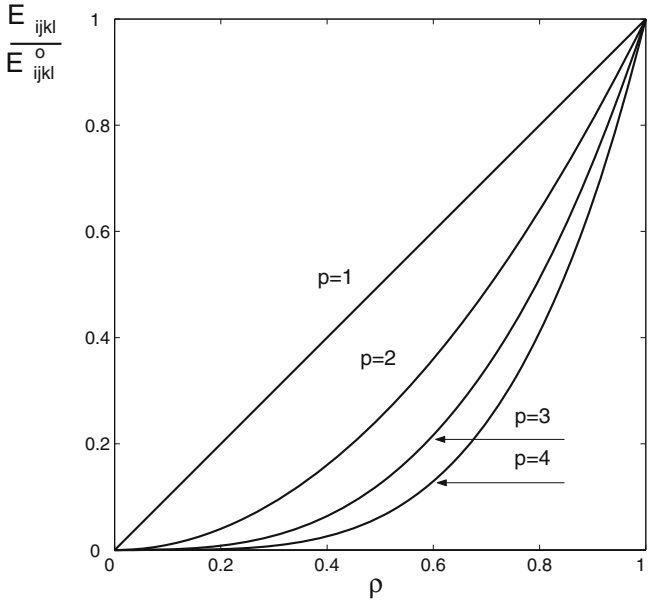

Fig. 4 Penalty coefficients for the components of the tensor E_{ijkl} as functions of the material density ρ (see Bendsøe and Sigmund 2002)

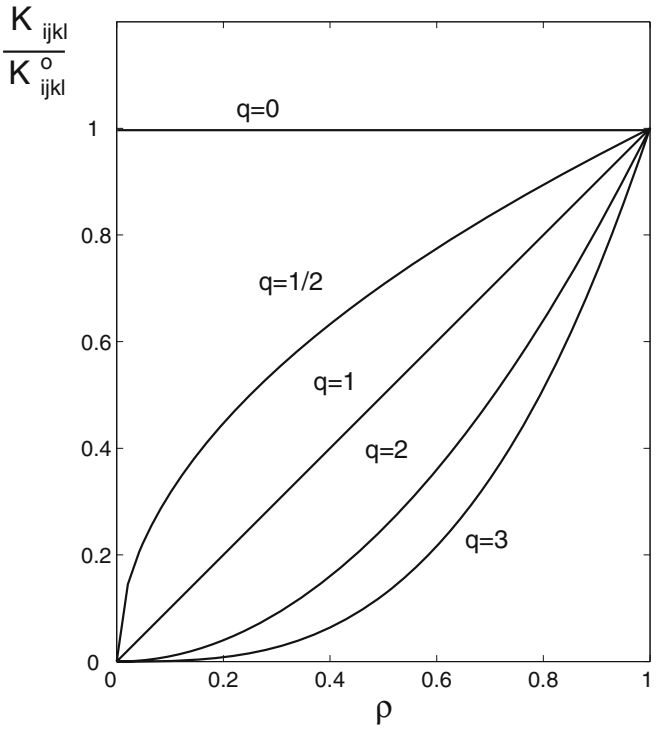

Fig. 5 Penalty coefficients for the components of the tensor K_{ijkl} as functions of the material density ρ

Therefore, the constitutive equations, written in matrix form, read:

$$[\,\sigma\,] = [\,\mathrm{E}\,]\,[\,\varepsilon\,], \tag{48}$$

$$[\,m\,] = [\,\mathrm{K}\,]\,[\,\chi\,]. \tag{49}$$

Explicitly:

$$\begin{bmatrix}\sigma_{11}\\ \sigma_{22}\\ \sigma_{12}\\ \sigma_{21}\end{bmatrix} = \begin{bmatrix}E_{1111} & E_{1122} & E_{1112} & E_{1121}\\ E_{2211} & E_{2222} & E_{2212} & E_{2221}\\ E_{1211} & E_{1222} & E_{1212} & E_{1221}\\ E_{2111} & E_{2122} & E_{2112} & E_{2121}\end{bmatrix}\begin{bmatrix}\varepsilon_{11}\\ \varepsilon_{22}\\ \varepsilon_{12}\\ \varepsilon_{21}\end{bmatrix},$$

$$\begin{bmatrix}m_{31}\\ m_{32}\end{bmatrix} = \begin{bmatrix}K_{3131} & K_{3132}\\ K_{3231} & K_{3232}\end{bmatrix}\begin{bmatrix}\chi_{31}\\ \chi_{32}\end{bmatrix}.$$

In matrix notation, the compatibility equations are:

$$\begin{bmatrix}\varepsilon_{11}\\ \varepsilon_{22}\\ \varepsilon_{12}\\ \varepsilon_{21}\end{bmatrix} = \begin{bmatrix}\partial_{x1} & 0\\ 0 & \partial_{x2}\\ 0 & \partial_{x1}\\ \partial_{x2} & 0\end{bmatrix}\begin{bmatrix}u_1\\ u_2\end{bmatrix} + \begin{bmatrix}0\\ 0\\ -1\\ +1\end{bmatrix}\begin{bmatrix}\phi_3\end{bmatrix}, \tag{50}$$

$$\begin{bmatrix}\chi_{31}\\ \chi_{32}\end{bmatrix} = \begin{bmatrix}\partial_{x1}\\ \partial_{x2}\end{bmatrix}\begin{bmatrix}\phi_3\end{bmatrix}, \tag{51}$$

where the following differential operators were introduced:

$$\bar{\mathrm{D}} = \begin{bmatrix}\partial_{x1} & 0\\ 0 & \partial_{x2}\\ 0 & \partial_{x1}\\ \partial_{x2} & 0\end{bmatrix}, \quad \tilde{\mathrm{D}} = \begin{bmatrix}0\\ 0\\ -1\\ +1\end{bmatrix}, \quad \hat{\mathrm{D}} = \begin{bmatrix}\partial_{x1}\\ \partial_{x2}\end{bmatrix}.$$

The equilibrium is given by:

$$\begin{bmatrix}\partial_{x1} & 0 & 0 & \partial_{x2} & 0 & 0\\ 0 & \partial_{x2} & \partial_{x1} & 0 & 0 & 0\\ 0 & 0 & +1 & -1 & \partial_{x1} & \partial_{x2}\end{bmatrix}\begin{bmatrix}\sigma_{11}\\ \sigma_{22}\\ \sigma_{12}\\ \sigma_{21}\\ m_{31}\\ m_{32}\end{bmatrix} + \begin{bmatrix}\mathrm{b}_1\\ \mathrm{b}_2\\ \mathrm{m}_3\end{bmatrix} = \begin{bmatrix}0\\ 0\\ 0\end{bmatrix}, \tag{52}$$

where the complete differential operator is:

$$\mathrm{D}^{\mathrm{T}} = \begin{bmatrix}\partial_{x1} & 0 & 0 & \partial_{x2} & 0 & 0\\ 0 & \partial_{x2} & \partial_{x1} & 0 & 0 & 0\\ 0 & 0 & +1 & -1 & \partial_{x1} & \partial_{x1}\end{bmatrix} = \begin{bmatrix}\bar{\mathrm{D}}^{\mathrm{T}} & \oslash\\ \tilde{\mathrm{D}}^{\mathrm{T}} & \hat{\mathrm{D}}^{\mathrm{T}}\end{bmatrix}.$$

In the former expression, $\oslash$ represents the null submatrix. The micropolar strain, microcurvature, and stress and couple stress fields, in terms of the generalized displacement vector, are written as:

$$[\varepsilon] = \bar{\mathrm{D}}\,[\,N^u\,]\,\mathbf{U}_D + \tilde{\mathrm{D}}\,[\,N^\phi\,]\,\mathbf{U}_R = \bar{\mathrm{B}}\,\mathbf{U}_D + \tilde{\mathrm{B}}\,\mathbf{U}_R\,, \tag{53}$$

$$[\chi] = \hat{\mathrm{D}}\,[\,N^\phi\,]\,\mathbf{U}_R = \hat{\mathrm{B}}\,\mathbf{U}_R\,, \tag{54}$$

$$[\sigma] = [\mathrm{E}]\;\bar{\mathrm{B}}\,\mathbf{U}_D + [\mathrm{E}]\;\tilde{\mathrm{B}}\,\mathbf{U}_R\,, \tag{55}$$

$$[m] = [\mathrm{K}]\;\hat{\mathrm{B}}\,\mathbf{U}_R. \tag{56}$$

The stiffness matrix of each finite element takes the form (see Providas and Kattis 2002):

$$\big[\,\mathrm{K}\,\big] = \begin{bmatrix}\bar{\mathrm{B}}^T\;[\mathrm{E}]\;\bar{\mathrm{B}} & \bar{\mathrm{B}}^T\;[\mathrm{E}]\;\tilde{\mathrm{B}}\\ \tilde{\mathrm{B}}^T\;[\mathrm{E}]\;\bar{\mathrm{B}} & \tilde{\mathrm{B}}^T\;[\mathrm{E}]\;\tilde{\mathrm{B}} + \hat{\mathrm{B}}^T\;[\mathrm{K}]\;\hat{\mathrm{B}}\end{bmatrix}. \tag{57}$$

The stiffness matrix can be decomposed in two parts corresponding to the tensors E_{ijkl} and K_{ijkl}:

$$\begin{aligned}[\mathrm{K}] &= \big[\mathrm{K}^{\mathrm{I}}\big] + \big[\mathrm{K}^{\mathrm{II}}\big]\\ &= \begin{bmatrix}\bar{\mathrm{B}}^T\,[\mathrm{E}]\,\bar{\mathrm{B}} & \bar{\mathrm{B}}^T\,[\mathrm{E}]\,\tilde{\mathrm{B}}\\ \tilde{\mathrm{B}}^T\,[\mathrm{E}]\,\bar{\mathrm{B}} & \tilde{\mathrm{B}}^T\,[\mathrm{E}]\,\tilde{\mathrm{B}}\end{bmatrix} + \begin{bmatrix}\oslash & \oslash\\ \oslash & \hat{\mathrm{B}}^T\,[\mathrm{K}]\,\hat{\mathrm{B}}\end{bmatrix}.\end{aligned} \tag{58}$$

Then, the optimization problem previously formulated (see 33) can be rewritten in discretized form as:

$$\begin{aligned}&\min_{\rho_e,u,\phi}\ \sum_{e=1}^{N}\left[(\mathbf{F^e})^{\mathbf{T}}\mathbf{U^e_D} + (\mathbf{M^e})^{\mathbf{T}}\mathbf{U^e_R}\right],\\ &\text{s.t.}:\ \left[\sum_{e=1}^{N}\left(\rho_e^p\,\left[\mathrm{K}^{\mathrm{I}}_{\mathrm{e}}\right] + \rho_e^q\,\left[\mathrm{K}^{\mathrm{II}}_{\mathrm{e}}\right]\right)\right]\mathbf{U} = \mathbf{F_G}\,,\\ &\qquad\sum_{e=1}^{N} A_e\,\rho_e\ \le \mathcal{V},\\ &\qquad 0 < \rho_{min} < \rho \le 1\,,\end{aligned} \tag{59}$$

where $\mathbf{F_G}$ denotes the vector of the generalized nodal forces:

$$\mathbf{F}_G^T = [\mathbf{F}\,,\mathbf{M}]\,. \tag{60}$$

The material penalization law considers the components E_{ijkl} and K_{ijkl} separately (see (39), (40), and (41)). Two different material interpolation methods are shown in Figs. 5 and 6 where the different penalization coefficients of translational and rotational tensors can be understood.

5 Examples

In this section, some examples obtained with the use of the proposed formulation are shown. The results are compared with the solutions of the same problems for a Cauchy continuum (with $E = 1$ and $\nu = 0.3$), that is, in absence of an intrinsic length scale. For all examples the material is assumed as micropolar, isotropic, and elastic, with Young's modulus $E_m = 1$ and Poisson's ratio $\nu_m = 0.3$. In the graphical representations of the optimal solutions, black and white are used to represent the density field where white means void ($\rho_{min} = 10^{-3}$) and black regions correspond to the base material ($\rho = 1$). For all examples the volume fraction is equal to 0.3. The first example is the classical end-loaded cantilever short beam (Fig. 6) with height/length = 2/5 and discretized with 200×80 four-node finite elements. The optimal solution for a Cauchy solid is shown in Fig. 7, where a truss-like configuration was obtained. Strongly different solutions are presented, for a micropolar solid, in Figs. 8 and 9. Figure 8

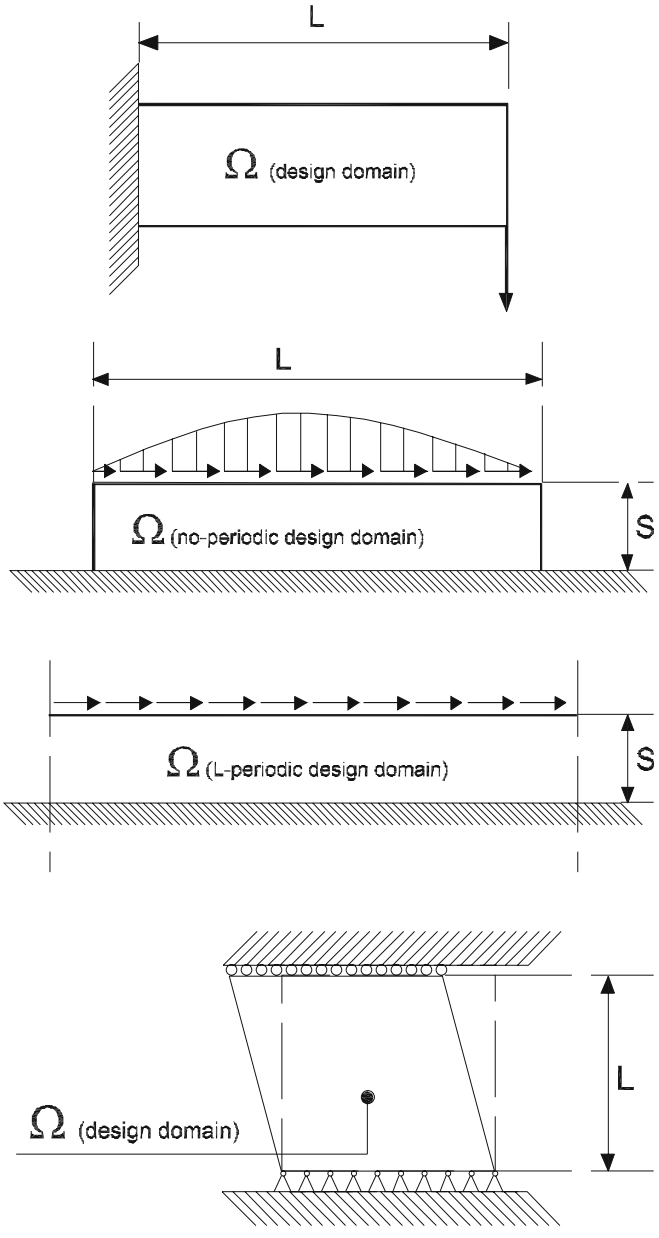

Fig. 6 Examples: short cantilever beam, structural interface subjected to shear load, periodic interface with displacements and rotations constrained at the bottom, and square element under a prescribed shear type deformation

presents optimal results for different values of the characteristic length for bending (ℓ_m). Figure 9 shows optimal configurations for various penalization coefficients associated with the rotational part of the micropolar stiffness tensor. The second example in Fig. 6 concerns a long strip of finite length made of a micropolar elastic material, clamped at the bottom, and subjected to a parabolic shear load at the top. The dimensions of the structure are such that the height/length ratio is equal to 1/5, and has been discretized by 300×60 four-node finite elements. This kind of structure is one of the simplest models adopted to simulate interfaces between solids.

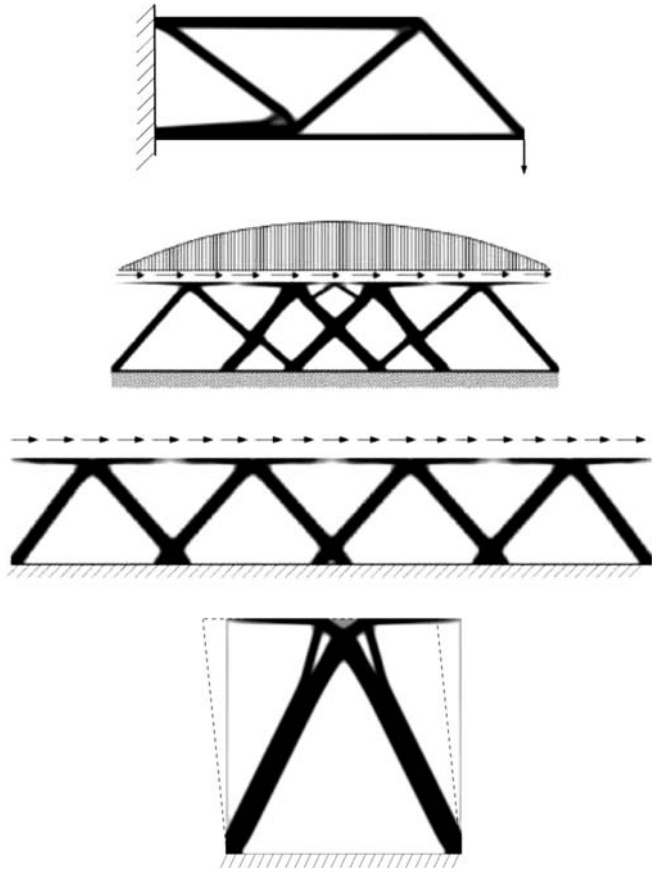

Fig. 7 Optimal solutions of the problems in this figure for a Cauchy solid: cantilever short beam, structural interface subjected to shear load, and square element under a shear type deformation

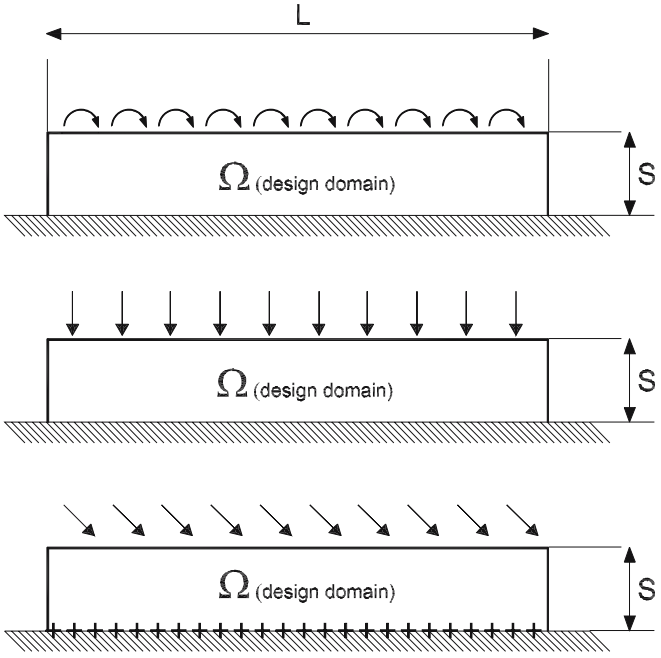

Fig. 8 Examples: interface problem with displacements, rotations, and microrotations constrained at the bottom and subjected to couple loads, uniform pressure, and inclined loads

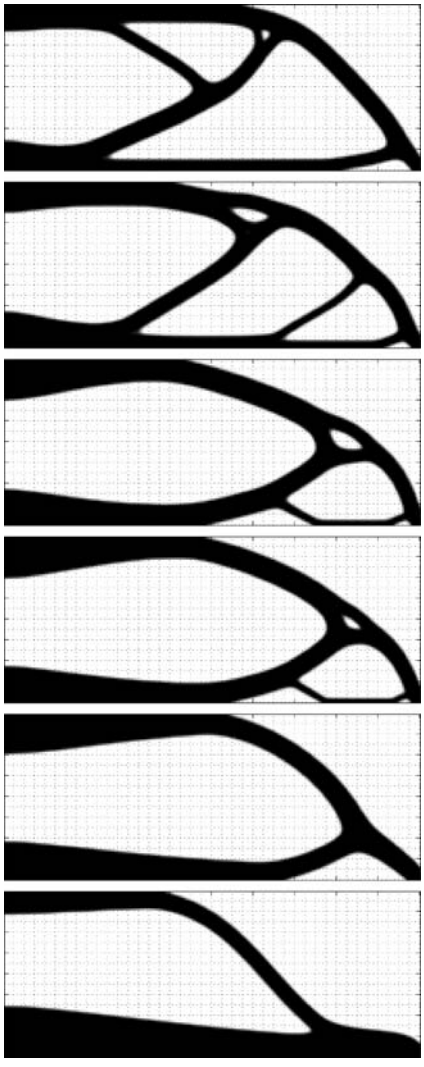

Fig. 9 Cantilever problem: Cosserat solid with coupling number $N_m = 0.9$, p=3, q=3; values of ℓ_m=0.05L, 0.10L, 0.15L, 0.25L, 0.30L, and 0.35L

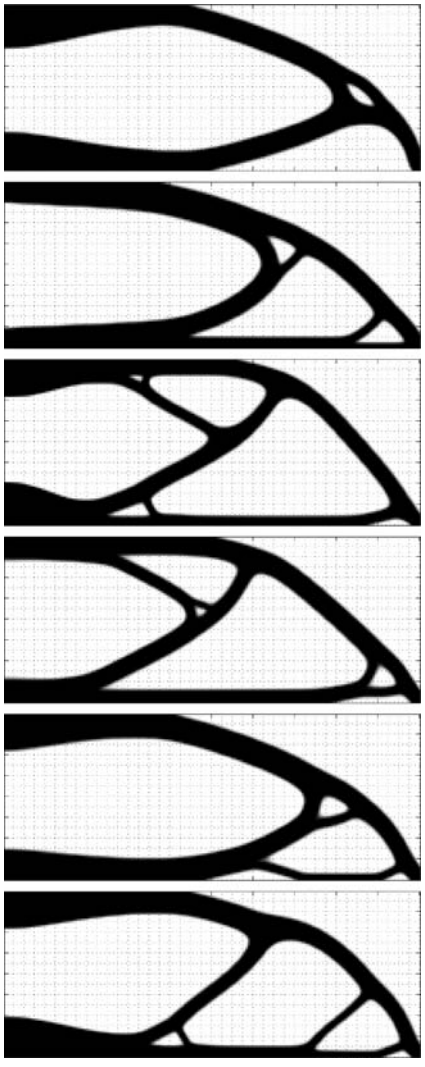

Fig. 11 Cantilever problem: Cosserat solid with coupling number $N_m = 0.8$, ℓ_m=0.015L, and p=3; values of q=0, 2, 3, 4, 5, and 10

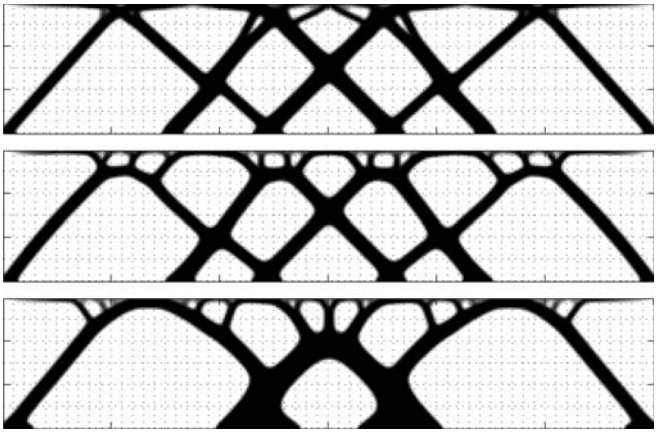

Fig. 10 Interface nonperiodic problem with coupling number $N_m = 0.8$; values of ℓ_m=0.025S, 0.5S, and 0.75S

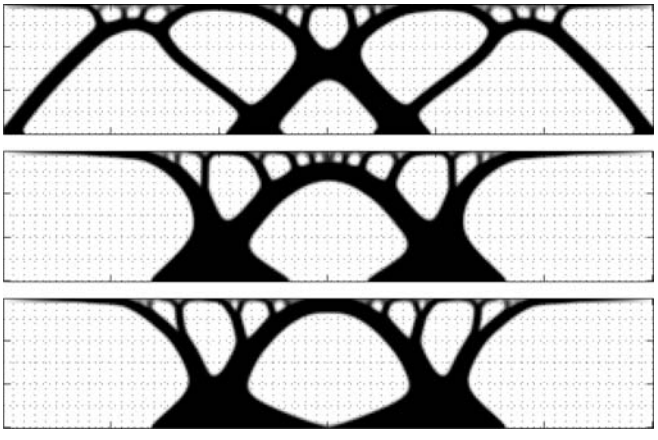

Fig. 12 Interface nonperiodic problem with coupling number N_m=0.8; values of ℓ_m=1.5S, 2.5S, and 3.5S

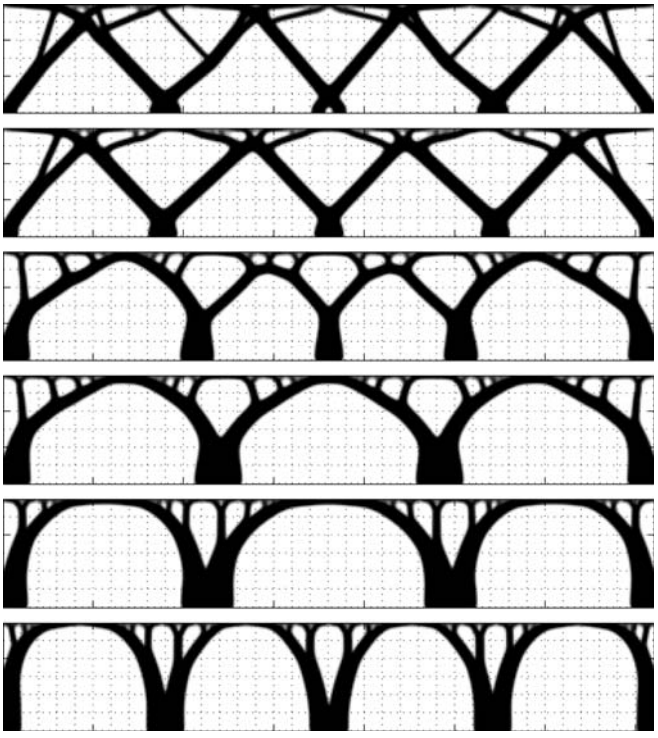

Fig. 13 Interface problem with coupling number N_m=0.8; values ofℓ_m=0.015S, 0.08S, 0.25S, 0.5S, 1.0S, and 1.5S

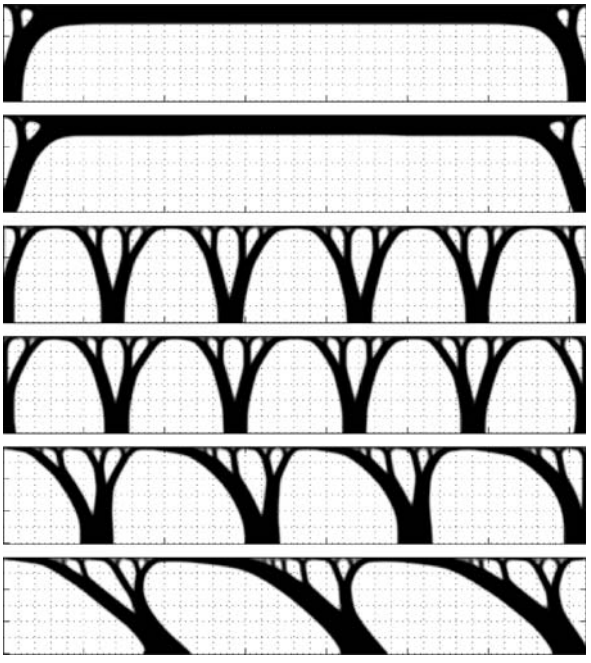

Fig. 15 Interface problem with coupling number 0.8. Examples 1 and 2 subjected to couple loads with p=3, q=3, and ℓ_m=1.0S with microrotations constrained and not contrained. Examples 3 and 4 subjected to pressure loads with p=3, q=3, and ℓ_m=1.5S with the same constraints. Examples 5 and 6 subjected to inclined loads with p=3, q=3, and ℓ_m=1.0S with the same constraints

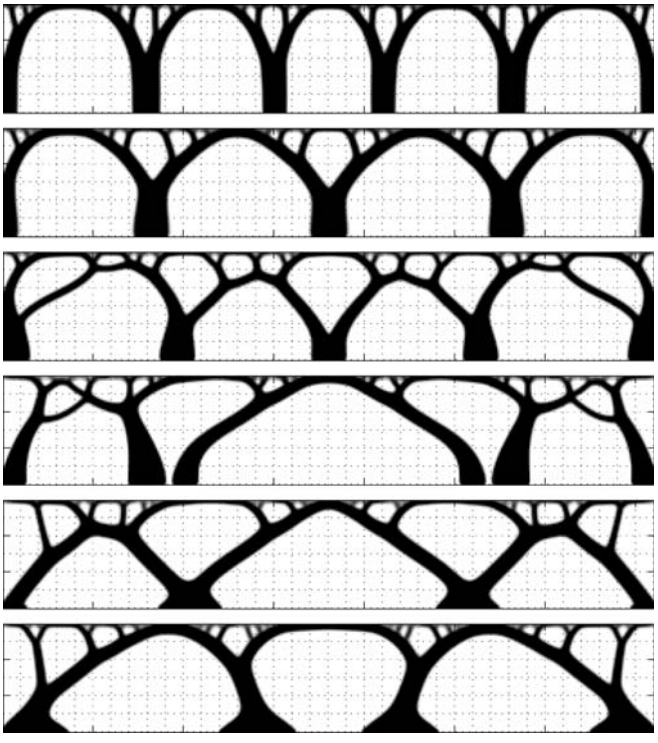

Fig. 14 Interface problem with coupling number N_m=0.8. Examples 1, 2, 3, and 4 with q=0, 1, 6, and 10, respectively, ℓ_m=3.0S, and p=3. Example 5 with ℓ_m=0.075S, p=3, q=3, and N_m=0.8 in the absence of microrotational constraints. Example 6 with ℓ_m=0.15S, p=3, q=3, and N_m=0.8 without microrotational constraints

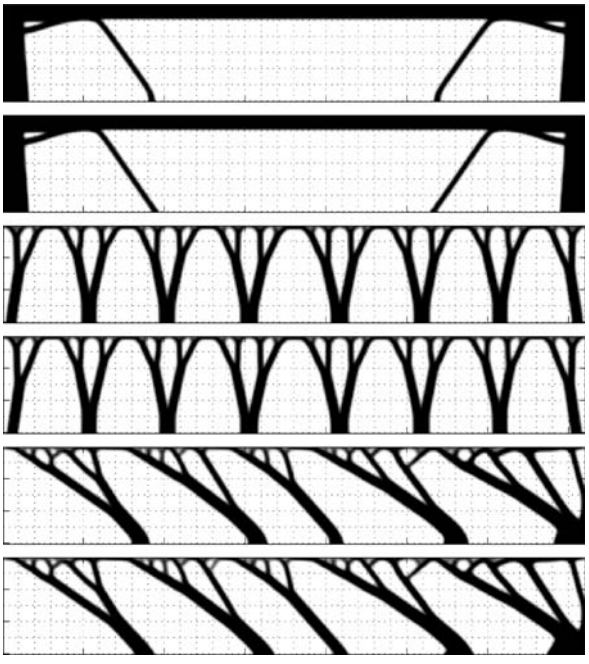

Fig. 16 Interface problem with coupling number 0.8. Examples 1 and 2 subjected to couple loads with p=3, q=3, and ℓ_m=0.08S with microrotations constrained and not constrained. Examples 3 and 4 subjected to pressure loads with p=3, q=3, and ℓ_m=0.08S with the same constraints. Examples 5 and 6 subjected to inclined loads with p=3, q=3, and ℓ_m=0.08S with the same constraints

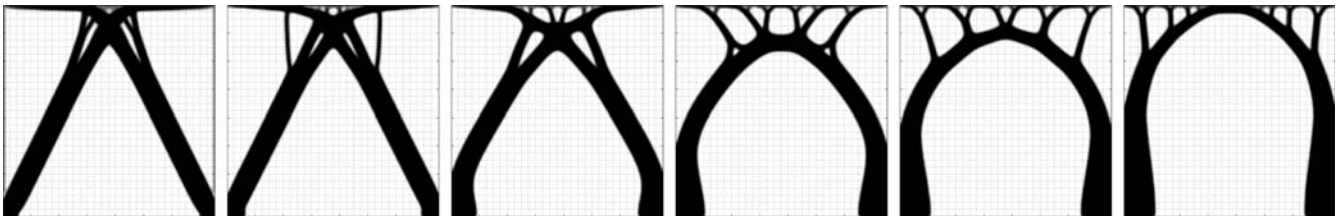

Fig. 17 Shear type deformation with coupling number 0.8, p=3, and q=3; values of ℓ_m=0.0067L, ℓ_m=0.033L, ℓ_m=0.133L, ℓ_m=0.2667L, ℓ_m=0.4000L, and ℓ_m=0.6667L

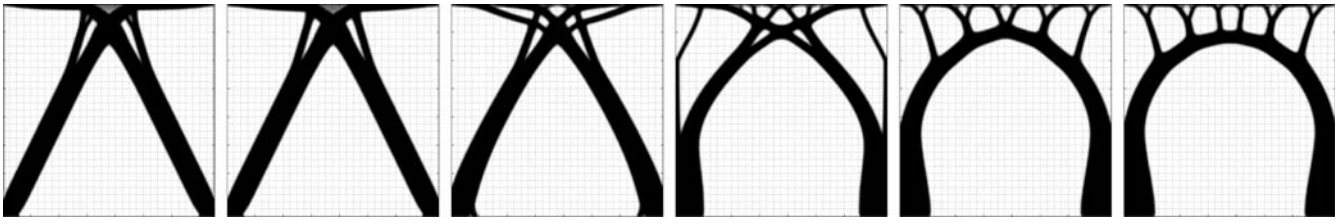

Fig. 18 Shear type deformation ℓ_m=0.4000L, p=3 and q=3; values of N_m=0.05, N_m=0.1, N_m=0.3, N_m=0.6, N_m=0.8, and N_m=0.9

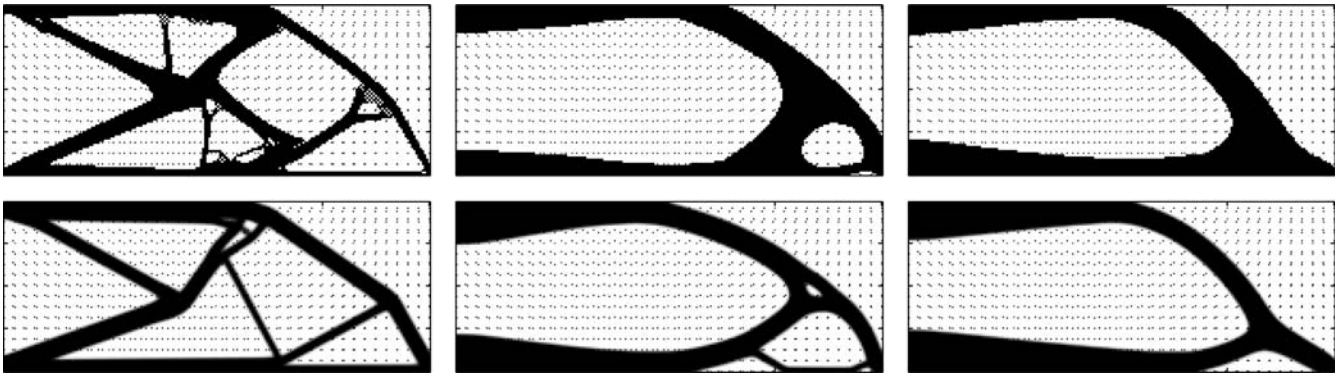

Fig. 19 Cantilever problem p=3, q=3, and N_m=0.8; discretized by four-node generalized isoparametric finite elements; values of ℓ_m=0.005L, ℓ_m=0.075L, and ℓ_m=0.25L with and without checkerboard control by filtering

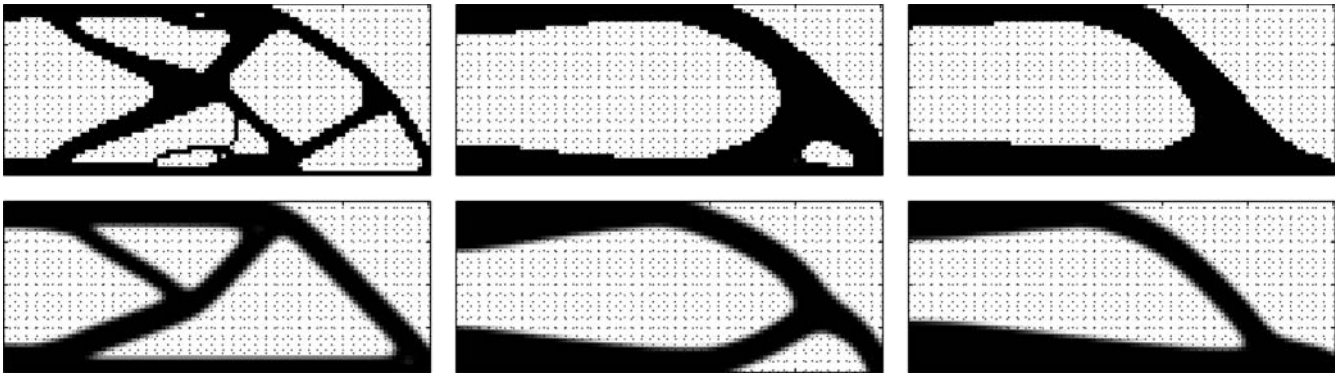

Fig. 20 Cantilever problem p=3, q=3, and N_m=0.8; discretized by eight-node generalized isoparametric finite elements; values of ℓ_m=0.005L, ℓ_m=0.075L, and ℓ_m=0.25L with and without checkerboard control by filtering

The optimal solutions of Figs. 10 and 11, obtained for a given coupling number and different values of the characteristic length of bending, clearly show that at the optimum the interface assumes a well-defined structural configuration. The optimal solution for the same interface problem, but not for a Cauchy solid, is given in the second picture of Fig. 7. The third example in Fig. 6 deals with a strip of infinite length clamped at the bottom and subjected to a constant shear force on the top. The optimal solutions are found for different values of the characteristic length (see Fig. 12) and for different penalization coefficients for the rotational components K_{ijkl} of the constitutive tensor and different microrotational constraints (see Fig. 13). The fourth example in Fig. 6 concerns a unit cell subjected to shear type deformation. The cell was discretized with 200×200 four node finite elements. The results of the optimization problem are shown in Fig. 14 and 15. In the first one the results for different values of the characteristic length of bending are shown, whereas in the second picture different values of the coupling number are taken into account. It may be interesting to observe for Fig. 15 that the formation of a fine substructure is related to large values of N_m, rather than to large values of ℓ_m. This effect is due to the fact that N_m governs the nonsymmetry of the constitutive response, while ℓ_m the rotational stiffness for applied couple-stresses. In Figs. 16 and 17, some optimal configurations of an infinite strip under different loading conditions and different constraints are shown (see Fig. 18 for static scheme). The examples presented show how the degree of connectivity of the optimal solutions strongly depend on the micropolar constitutive parameters (characteristic length of bending and coupling number). Finally, Figs. 19 and 20 present optimized cantilever beams obtained by using four and eight isoparametric finite elements with and without linear filtering of the sensitivities (see Bendsøe and Sigmund 2002). In the examples presented in this section, which show different rotational penalization coefficients K_{ijkl} (Figs. 9 and 13), the solutions of maximum stiffness correspond to $q = 0$. In this case the penalization acts only on the translational part, i.e.:

$$E_{ijkl}(\mathbf{x}) = \rho(\mathbf{x})^p E^0_{ijkl}\,, \qquad \text{with } p \geq 1\,, \tag{61}$$

$$K_{ijkl}(\mathbf{x}) = K^0_{ijkl}\,. \tag{62}$$

The assumed values of the penalization parameter q admit a mechanical interpretation. In particular, the case $q = 0$ corresponds to a characteristic length for bending dependent only on the dimensions of the representative volume element (RVE) but not on the relative material density. On the other hand, when $q \neq 0$ the characteristic length for bending depends on the RVE relative material density.

6 Conclusions and perspectives

In this paper, the topology optimization for maximum stiffness applied to micropolar (and, in particular, to Cosserat) solids was formulated and solved. Several examples of application were shown, and compared with those obtained (with the same amount of material available) for Cauchy solids. The results on the one hand show that for the Cauchy continuum model the optimal solutions are shaped as truss-like structures, on the other hand, in the case of Cosserat continua, the optimized structures are much more complex and characterized by attractive shapes. The mechanical model and the geometry of the design domains in the examples presented in this paper find interesting applications in the fields of structural interfaces and mechanics of biological materials. In the future the model can be, with some effort, enriched by first including material anisotropies and then considering other mechanical models like those of micromorphic, microstructured, and noncentrosymmetric materials.

Acknowledgements The authors gratefully acknowledge the financial support from MIUR-PRIN 2004, *Microstructural problems and models: applications in structural and civil engineering*. The authors are deeply indebted to Prof. Niels Olhoff for his useful comments on the first version of this paper. A special thank you also goes to Prof. John E. Taylor for directing the authors to the present topic.

References

Bendsøe MP, Sigmund O (2002) Topology optimization: theory, methods and applications. Springer, Berlin Heidelberg New York

Chen Y, Lee JD, Eskandarian A (2004) Atomistic viewpoint of the applicability of microcontinuum theories. Int J Solids Struct 41: 2085–2097

Cheng KT, Olhoff N (1982) Regularized formulation for optimal design of axisymmetric plates. Int J Solids Struct 18:153–169

Eringen AC (1966) Linear theory of micropolar elasticity. J Math Mech 15(6):909–923

Eringen AC (1999) Microcontinuum field theories, vol 1. Springer, Berlin Heidelberg New York

Eschenauer HA, Olhoff N (2001) Topology optimization of continuum structures: a review. Appl Mech Rev 54(4):331–390

Fatemi J, van Keulen F (2003) Identification of elastic constants of micropolar solids using an optimization approach. WCSMO5, Venice Italy, 2003

Fatemi J, Van Keulen F, Onck PR (2002) Generalized continuum theories: application to stress analysis in bone. Meccanica 37:385–396

Gauthier RD, Jahsman WE (1975) A quest for micropolar elastic constants. J Appl Mech ASME 42:369–374

Hutapea P, Qiao P (2001) Micropolar in-plane shear and rotation moduli of unidirectional fiber composites with fiber-matrix interfacial debonding. J Comp Mech 36(11)

Koiter WT (1964) Couple stress in the theory of elasticity, parts I and II. Mech 67:17–44

Lakes RS (1986) Experimental microelasticity of two porous solids. Int J Solids Struct 22:55–63

Lakes RS (1995) Experimental methods for study of Cosserat elastic solids and other generalized elastic continua. In: Mühlhaus H (ed) Continuum models for materials with micro-structure. Wiley, New York, pp 1–25

Lakes RS, Benedict RL (1982) Noncentrosymmetry in micropolar elasticity. Int J Eng Sci 20(10):1161–1167
Novacki W (1986) Theory of asymmetric elasticity. Pergamon, New York
Providas E, Kattis MA (2002) Finite element method in plane Cosserat elasticity. Comp Struct 80:2059–2069
Rosenberg J, Cimrman R (2001) Microcontinuum in biomechanical medelling. Mathematics and Computers in simulation. Proceedings of the Conference Modelling, Plzen, 2001
Walsh SDC, Tordesillas A (2003) A thermomechanical approach to the development of micropolar costitutive models of granular media. Acta Mech 167(3–4):145–169